Fine-tuning of a ferrocene|porphyrin|ITO redox cascade for efficient sequential electron transfer commenced by an S_2 photoexcited special-pair mimic†

Mitsuhiko Morisue,‡ Dipak Kalita, Noriko Haruta and Yoshiaki Kobuke*

Received (in Cambridge, UK) 15th January 2007, Accepted 12th February 2007
First published as an Advance Article on the web 7th March 2007
DOI: 10.1039/b700632b

A systematic series of ferrocene/porphyrin redox cascade architectures was assembled through a slipped-cofacial porphyrin dimer on ITO electrode in optimizing the anodic photocurrent generation to perform the highest quantum yield compared to reported values on ITO electrodes.

The excellent conversion of light energy in natural photosynthetic systems has prompted many scientists to design energy and/or electron transfer systems.[1] In recent decades, elaborate cascade architectures of appropriate redox components on a conductive electrode surface have been constructed using molecular systems with efficient interfacial electron transfer.[2–5] One successful strategy for the generation of an anodic photocurrent has employed a cascade architecture composed of porphyrin|fullerene|ITO (tin-doped indium oxide) system based on the efficient charge-separation between the porphyrin photosensitizer and a fullerene electron acceptor.[3,4] Alternatively, the close contact of the photosensitizer on an ITO electrode surface is effective in improving the generation of an anodic photocurrent in conjunction with the n-type semiconductor character of ITO.[6] The preferential charge injection to the conduction band (CB) of the ITO anode before vibrational relaxation, *i.e.*, hot injection, is an attractive process for constructing an efficient artificial photosynthetic reaction centre.

In bacterial photosynthetic reaction centers, the primary electron donor constitutes a slipped-cofacial dimer of chlorophyll, the so-called "special pair".[7] Our strategy for constructing an artificial photosynthetic reaction center emulates the configuration of a special pair using an imidazolyl-to-zinc complementary coordination in an imidazolylporphyrinatozinc unit, Zn(ImP).[8] A study using this model elucidated that the slipped-cofacial configuration was a functional key for accelerating the charge-separation, while decelerating the charge-recombination due to the small reorganization energy.[9] Our trial using a porphyrin dimer-immobilized ITO succeeded in achieving an efficient electron transfer from the S_2 photoexcited state of the cofacial dimer to the CB of the ITO electrode.[6] The hot injection before internal conversion exhibited a relatively high quantum yield of 15% for anodic photocurrent generation. This was achieved by the effect of the slipped-cofacial dimer combined with the phosphonate-anchor on the ITO without an insulation layer. The construction of a redox cascade on the electrode surface was our aim to further improve the conversion of solar energy.

Herein, we demonstrate the first systematic optimization of a redox cascade on a conductive surface for the generation of a photocurrent using a modular self-organization methodology, *i.e.*, a series of ferrocene|porphyrin|ITO redox cascades, Zn(ImPD)-|Zn(ImPPO$_3$)|ITO (Fig. 1). The dissociation/organization of Zn(ImP)s by the addition/removal of a coordinating ligand provides a facile methodology for the formation of a heterogeneous dimer on a Zn(ImP)-assembled ITO surface.[6,10] The Zn(ImPPO$_3$) is first assembled as a monolayer on the ITO electrode, and this modification turns out to be appropriate for hot injection, compared to a thiolate or isophthalate linker.[6] A systematic series of ferrocene-homologue-tethered Zn(ImP)[11] is then assembled on the Zn(ImPO$_3$) scaffold, Zn(ImPD)-|Zn(ImPPO$_3$)|ITO, which constructs the porphyrin heterodimer redox cascade on the ITO. The structural elucidation of the electrode surface was carried out using X-ray photoelectron spectroscopy (XPS). Based on the Fe 2p/P 2p ratio obtained, 40% of the surface-confined porphyrin had been converted to the Zn(ImPFc)|Zn(ImPPO$_3$)|ITO heterodimer. The XPS deconvoluted profiles for the N 1s region also gave a similar estimation. This

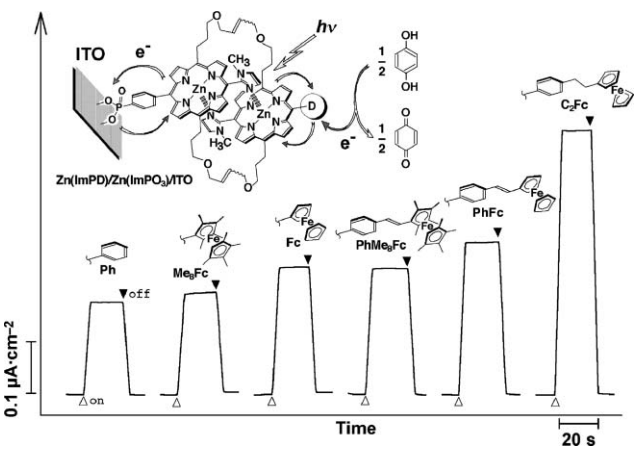

Fig. 1 Photocurrent response during on/off cycle of excitation light at 410 nm (98.2 μW cm^{-2}) for Zn(ImPD)|Zn(ImPPO$_3$)|ITO (where, on passing from left to right, D = Ph, Me$_8$Fc, Fc, PhMe$_8$Fc, PhFc and C$_2$Fc) at a potential of 100 mV *vs.* Ag/AgCl in 50 mM H_2Q (pH = 6.2). The inset shows a schematic illustration of the structure of Zn(ImPD)|Zn(ImPPO$_3$)|ITO.

Graduate School of Materials Science, Nara Institute of Science and Technology, Ikoma, 630-0192, Japan. E-mail: kobuke@ms.naist.jp; Fax: (+81)743-72-6119

† Electronic supplementary information (ESI) available: XPS, CV, UV-vis and photocurrent action spectra. See DOI: 10.1039/b700632b

‡ Present Address: Faculty of Biomolecular Engineering, Kyoto Institute of Technology, Matsugasaki, Sakyo-ku, Kyoto 606-8585, Japan. E-mail: morisue@kit.ac.jp.

Table 1 Redox potentials of the ferrocenyl terminals in CH_2Cl_2,[11] and the quantum yield of the anodic photocurrent of Zn(ImPD)|Zn(ImPPO$_3$)|ITO excited at 410 nm at potentials of 100 and 200 mV *vs.* Ag/AgCl

Zn(ImPD)	$D^{+/0}$	Φ_{410}/Φ_{550} (%) at 100 mV	Φ_{410} (%) at 200 mV
Zn(ImPPh)	—	10/4.3	13
Zn(ImPMe$_8$Fc)	0.05	11/8.0	14
Zn(ImPFc)	0.46	14/6.5	18
Zn(ImPPhMe$_8$Fc)	0.08	14/4.5	16
Zn(ImPPhFc)	0.45	16/4.5	20
Zn(ImPC$_2$Fc)	0.45	27/7.0	40

evaluation is in line with the case of Zn(ImPPh)|Zn(ImPPO$_3$)|ITO estimated from the N 1s/P 2p ratio.[6] The absorption spectra showed almost the same properties in all the runs on a series of Zn(ImPPO$_3$)|ITO and successive Zn(ImPD)|Zn(ImPPO$_3$)|ITO samples. Therefore, the terminal electron donor groups were immobilized on the ITO surface with a similar surface coverage. The redox potentials of the ferrocenyl terminals should appear around 0.45 and 0.05 V for the non-substituted (Fc) and octamethyl-substituted (Me$_8$Fc) cases, respectively (see Table 1).[11] However, no redox peaks from the ferrocenyl terminal were observed for Zn(ImPD)-modified ITO in the desired region; instead, the oxidation waves of the porphyrin were enhanced. Therefore, no response of the ferrocenyl terminal accounts for the segregation from the ITO surface by the slipped-cofacial porphyrin dimer.

A photocurrent was observed on irradiation of the Zn(ImPD)|Zn(ImPPO$_3$)|ITO surfaces exposed to a deoxygenated aqueous electrolyte (pH = 6.2) containing hydroquinone (H_2Q, 50 mM) acting as the sacrificial electron donor. Fast photocurrent responses were observed according to an induced on/off light irradiation cycle (Fig. 1). A highly efficient photocurrent was observed when the Soret band (S_2) was excited (Fig S3, ESI†). On the other hand, excitation of the Q-band (S_1) generated a relatively small anodic photocurrent. This difference is ascribable to the hot injection from the S_2* state to the CB and from the S_1* state to the Fermi level.[6]

We will discuss the generation of a photocurrent by excitation at the S_2 band. When the ferrocenyl group is introduced on the molecular terminal, the anodic photocurrent is enhanced, depending on the redox potential and the spacer unit of the ferrocenyl terminal, even though these porphyrin heterodimers show similar extinction values on the ITO electrode (Fig. 1). Considering the fact that the ferrocenyl terminals improve the overall generation of an anodic photocurrent, the ferrocenyl terminals relay the electron flow from the bulk H_2Q to the porphyrin unit, and subsequently to the ITO electrode. Two possible processes can account for this increase: (1) the hot injection from the S_2* state to the CB and the subsequent hole shift to the ferrocenyl terminal assists the reduction of the porphyrin cation by the bulk H_2Q, and (2) the reductive electron transfer from the ferrocenyl terminal drives the electron transfer from the porphyrin anion radical to the ITO acceptor level. Although it is difficult to choose which of these alternative mechanisms occur, the former process is more likely because, in general, Zn porphyrins are good electron donors. The following considerations support the mechanism.

In regards to the distance of the charge-separated ion pair ($ITO^-\cdots D^+$), the directly connected ferrocenium cation (D = Fc) is the most susceptible to both a hole shift and a charge recombination. A separation of the ferrocenyl terminal from the ITO surface lowers the frequency of charge recombination. When the ferrocenyl terminal is connected *via* a π-conjugated linkage (D = PhFc), then the effect of the increased separation of the ferrocenyl terminals suppress the competitive backward process, although this is still modest (Scheme 1(b)). The distal electron donor group without π-conjugation (D = C_2Fc) is the most advantageous option for further enhancement of the anodic photocurrent to give the best result among the options examined (Fig. 1 and Table 1). No significant fluorescence quenching in an isotropic medium only in this last case indicates that no electron transfer from the ferrocene to the photoexcited porphyrin occurs. Therefore, supplying the electron from the ferrocene to the porphyrin cation immediately after the hot injection enhances the anodic photocurrent (Scheme 1(a)).

The photocurrent properties reveal the effect of the redox potential of the ferrocenyl terminal. A large potential gap should lead to a more effective electron transfer from the Me$_8$Fc and PhMe$_8$Fc terminals to the porphyrin cation than for the cases of Fc and PhFc terminals, due to the higher oxidation potential of the former terminals. However, the photocurrent generation characteristics showed the reverse tendency. The mismatching of the redox potential from bulk H_2Q (0.15 V *vs.* Ag/AgCl at pH = 6.2) to Me$_8$Fc made reduction relatively less significant (Scheme 1(c)). Judging from the fact that the Me$_8$Fc and PhMe$_8$Fc terminals are still effective for improving the generation of an anodic photocurrent, the reduction of the outer ferrocenyl terminal by the bulk H_2Q is sufficiently fast. In contrast, the Fc, PhFc, and C_2Fc terminals provide a downhill redox gradient to relay a smooth sequential electron transfer from the H_2Q to the porphyrin

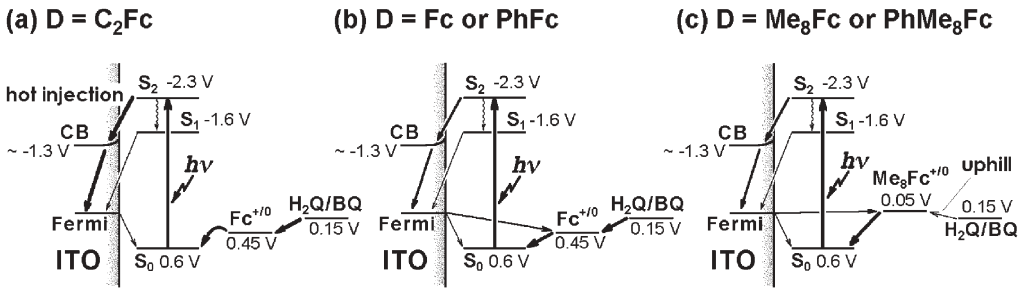

Scheme 1 Potential diagrams for D = C_2Fc (a), for D = Fc or PhFc (b), and for Me$_8$Fc or PhMe$_8$Fc (c) at anodic potentials when the Soret (S_2) band is excited.

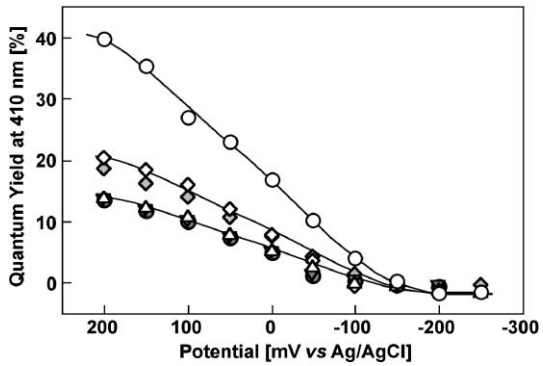

Fig. 2 Dependence of the anodic quantum yield of Zn(ImPD)-|Zn(ImPPO$_3$)|ITO on the potential, excited at 410 nm (*I–V* characteristics) for D = C_2Fc (open circles), D = PhFc (open squares), D = Fc (filled squares), D = PhMe$_8$Fc (open triangles), D = Me$_8$Fc (filled triangles), and D = Ph (filled circles).

(Scheme 1(a) and (b)). The smooth redox gradient over the entire circuit leads to an efficient electron transfer.

The variation in the potential of the ITO electrode modulates the Fermi level, and concomitantly, the CB of the acceptor level.[12] The photocurrent quantum yield was moderately improved when a higher anodic potential was applied. Each ferrocenyl terminal showed a similar trend in its *I–V* characteristics (Fig. 2). The difference in the oxidation potentials of Fc, PhFc, and C_2Fc, and those of Me$_8$Fc and PhMe$_8$Fc should be noted. If the electron transfer step from the ferrocenyl terminal to the porphyrin is critical in generating an anodic photocurrent, then the Me$_8$Fc and PhMe$_8$Fc terminals are expected to be more effective than the Fc and PhFc terminals, particularly under low bias conditions. However, the former *I–V* characteristics did not exceed the latter *I–V* characteristics, even under low bias potentials. Therefore, the primary electron transfer step is dominated by the hot injection from the S_2* photoexcited state to the CB. Most characteristically, the quantum yield for the anodic photocurrent reached 40% for Zn(ImPC$_2$Fc)|Zn(ImPPO$_3$)|ITO at a potential of 200 mV. To our best knowledge, this tailored cascade has realized the highest quantum yield for the generation of an anodic photocurrent on an ITO electrode.[3–5] The key functions involve the hot injection from the S_2 state of the photoexcited slipped-cofacial porphyrin dimer deposited on the ITO surface to its CB, and the subsequent charge shift onto the distal ferrocenyl terminal.

Combining the above results, the first assumption is most likely pertinent to the mechanism. In contrast to the hot injection from the S_2* state to the CB, injection from the S_1 state to the Fermi level provides a small photocurrent (Table 1). In this case, the Fermi level easily discharges the electron once it was injected from the S_1 state, unlike the CB with a band-bending structure acting as the barrier against the back electron transfer process.[6] This comparison emphasizes the advantage of the hot injection from the S_2* state to the CB.

In conclusion, we have succeeded in developing a modular self-organization methodology for optimizing a redox cascade using a slipped-cofacial dimer of imidazolylporphyrinatozinc as the key element. The artificial reaction center comprised of a "special pair"-mimic to achieve a markedly high quantum yield for the generation of an anodic photocurrent compared to previously reported values. The systematic optimization of the ferrocene|porphyrin|ITO redox elements shows that a sophisticated arrangement of the redox cascade is crucial for the efficient generation of a photocurrent by the rapid photooxidation of a special pair mimic, followed by a smooth hole shift to the distal ferrocenyl terminal. We believe that the slipped-cofacial configuration of the porphyrin dimer is endowed with a small driving force for the oxidative electron transfer reaction, and is certainly a powerful unit for the conversion of solar energy.

We gratefully acknowledge the financial support of this work by Grant-in-Aids for Scientific Research (A) (No 15205020) from Ministry of Education, Culture, Sports, Science and Technology, Japan (Monbu Kagakusho).

Notes and references

1 (*a*) T. Matsuo, *J. Photochem.*, 1985, **29**, 41; (*b*) M. R. Wasielewski, *Chem. Rev.*, 1992, **92**, 435; M. R. Wasielewski, *J. Org. Chem.*, 2006, **71**, 5051; (*c*) D. Gust, T. A. Moore and A. L. Moore, *Acc. Chem. Res.*, 2001, **34**, 40; (*d*) H. Imahori, *J. Phys. Chem. B*, 2004, **108**, 6130.
2 SAM|Au: (*a*) K. Uosaki, T. Kondo, X.-Q. Zhang and M. Yanagida, *J. Am. Chem. Soc.*, 1997, **119**, 8367; (*b*) H. Imahori, H. Norieda, H. Yamada, Y. Nisimura, I. Yamazaki, Y. Sakata and S. Fukuzumi, *J. Am. Chem. Soc.*, 2001, **123**, 100; (*c*) K.-S. Kim, M.-S. Kang, H. Ma and A. K.-Y. Jen, *Chem. Mater.*, 2004, **16**, 5058.
3 SAM|ITO: (*a*) H. Imahori, M. Kimura, K. Hosomizu, T. Sato, T. K. Ahn, S. K. Kim, D. Kim, Y. Nishimura, I. Yamazaki, Y. Araki, O. Ito and S. Fukuzumi, *Chem. Eur. J.*, 2004, **10**, 5111; (*b*) Y.-J. Cho, T. K. Ahn, H. Song, K. S. Kim, C. Y. Lee, W. S. Seo, K. Lee, S. K. Kim, D. Kim and J. T. Park, *J. Am. Chem. Soc.*, 2005, **127**, 2380.
4 Layer-by-layer|ITO: (*a*) A. Ikeda, T. Hatano, S. Shinkai, T. Akiyama and S. Yamada, *J. Am. Chem. Soc.*, 2001, **123**, 4855; (*b*) D. M. Guldi, I. Zilbermann, G. Anderson, A. Li, D. Balbinot, N. Jux, M. Hatzimarinaki, A. Hirsch and M. Prato, *Chem. Commun.*, 2004, 726.
5 Langmuir–Blodgett films: (*a*) M. Fujihira, K. Nishiyama and H. Yamada, *Thin Solid Films*, 1985, **132**, 77; (*b*) A. Aoki, Y. Abe and T. Miyashita, *Langmuir*, 1999, **15**, 1463.
6 M. Morisue, N. Haruta, D. Kalita and Y. Kobuke, *Chem. Eur. J.*, 2006, **12**, 8123.
7 J. Deisenhofer, O. Epp, K. Miki, H. Huber and H. Michel, *J. Mol. Biol.*, 1984, **180**, 385.
8 (*a*) Y. Kobuke and H. Miyaji, *J. Am. Chem. Soc.*, 1994, **116**, 4111; (*b*) Y. Kobuke, *Eur. J. Inorg. Chem.*, 2006, 2333.
9 H. Ozeki, A. Nomoto, K. Ogawa, Y. Kobuke, M. Murakami, K. Hosoda, M. Ohtani, S. Nakashima, H. Miyasaka and T. Okada, *Chem. Eur. J.*, 2004, **10**, 6393.
10 M. Morisue, S. Yamatsu, N. Haruta and Y. Kobuke, *Chem. Eur. J.*, 2005, **11**, 5563.
11 D. Kalita, M. Morisue and Y. Kobuke, *New J. Chem.*, 2006, **30**, 77.
12 S. M. Sze, *Physics of Semiconductor Devices*, Wiley, New York, 2nd edn, 1981.

